IOP Publishing | Astro Ltd Laser Physics

Laser Phys. **29** (2019) 096001 (8pp) https://doi.org/10.1088/1555-6611/ab342d

# Evaluation of the possibility of ignition of a hydrogen–oxygen mixture by erosive flame of the impulse laser

**Victor V Kuzenov**[1,2] **and Sergei V Ryzhkov**[1]

[1] Bauman Moscow State Technical University, 2nd Bauman Street, 5, 1. Moscow 105005, Russia
[2] Dukhov Research Institute of Automatics (VNIIA), Sushchevskaya str. 22, Moscow 127055, Russia

E-mail: svryzhkov@bmstu.ru

Received 31 January 2019
Accepted for publication 17 July 2019
Published 9 August 2019

**Abstract**

The paper presents the mathematical model of combustion initiation in a mixture of hydrogen and oxygen gases (oxyhydrogen) by a laser flare created near a metal barrier. For numerical resolution of the 'hyperbolic' part of Reynold's equations system, we give a new nonlinear quasimonotone compact polynomial difference scheme of improved accuracy. Calculations of all the main parameters: the laser flare, the heating of the metal barrier, and the combustion processes in the hydrogen–oxygen system are performed.

Keywords: pulsed Nd laser, ignition, mathematical model, numerical experiment, oxyhydrogen

(Some figures may appear in colour only in the online journal)

## 1. Introduction

Plasma formation that appears above the surface of a metal barrier, or directly in a gaseous substance as a result of the action of laser radiation, can be used to ignite a combustible mixture in perspective aircraft engines, as well as for creating laser plasmatrons. We also note that laser radiation and the associated volumetric energy release in a definite region of the supersonic flow can allow us to change the flow structure (a system of shock waves interacting with each other) in the desired direction.

From the viewpoint of numerical simulation, the task is rather complicated. Here we note its multicomponent nature, the high rigidity of chemical kinetic equations, etc [1, 2]. The complexity of the problem is also associated with a sharp temperature dependence of the chemical rate and a strong change in the density of the gas mixture due to a change in the average molecular weight. To overcome these difficulties, both significant computing power and the development of special algorithms are required.

## 2. Task and model

The mathematical model of the processes occurring in laser plasma is based on the multicomponent Reynolds radiation equations taking into account spontaneous electromagnetic fields and the turbulence of the plasma. A special feature of this model is the account and description of the contact boundary motion that separate the substance's plasma of the metal barrier and the surrounding gas.

To solve this system of equations using a finite-difference method, it is convenient to introduce a coordinate transformation of the form: $r = r(\xi, \eta, \zeta)$, $z = z(\xi, \eta, \zeta)$, $\varphi = \varphi(\xi, \eta, \zeta)$. When the coordinates of the grid nodes in the computational domain are known in physical space, $\xi$, $\eta$, $\zeta$, the metric coefficients in the general case, can be found by numerical differentiation.

Plasma dynamic processes occurring in laser plasma can be determined using a system of equations for viscous thermal equilibrium radiation plasma dynamics. In dimensionless variables this system of equations takes the following form:

 

$$\frac{\partial \rho c_i}{\partial t} + Div\left(\rho c_i \vec{V}\right) = -\alpha \frac{\rho c_i u}{r} + Div\left(\rho D_i \nabla c_i\right) + \left(\frac{\partial \rho c_i}{\partial t}\right), \quad \frac{\partial \rho}{\partial t} + Div\left(\rho \vec{V}\right) = -\alpha \frac{\rho u}{r},$$
$$\frac{\partial \rho u}{\partial t} + Div\left(\rho u \vec{V}\right) = -\xi_r \frac{\partial P}{\partial \xi} - \eta_r \frac{\partial P}{\partial \eta} - \alpha \frac{\rho u^2}{r} + \frac{S_r}{\mathrm{Re}}, \frac{\partial \rho \mathrm{v}}{\partial t} + Div\left(\rho \mathrm{v} \vec{V}\right) = -\xi_z \frac{\partial P}{\partial \xi} - \eta_z \frac{\partial P}{\partial \eta} - \alpha \frac{\rho u \mathrm{v}}{r} + \frac{S_z}{\mathrm{Re}}$$
$$\frac{\partial \rho e}{\partial t} + Div\left(\rho e \vec{V} + \sum \vec{q}_i\right) = -\frac{P}{J} Div\left(\vec{V}\right) - \alpha \frac{Pu}{r} - \alpha \frac{\rho e u}{r} + \frac{S_e}{\mathrm{Re}} + D$$
$$S_e = \mu_{\sum} D + \frac{\gamma}{\mathrm{Pr}} div\left(\lambda_{\sum} gradT\right) + \frac{\mathrm{Re}\, t_*}{\rho_* e_*} Q_L,$$
$$D = \sum_i h_i \frac{t_*}{e_*} Div\left(\rho D_i \nabla c_i\right), \quad Div\left(\right) = \frac{1}{J}\frac{\partial (J)}{\partial \xi} + \frac{1}{J}\frac{\partial (J)}{\partial \eta},$$

where the quantities $S_r, S_z$ mathematically describe the forces [3, 4] that arise in the laser flare due to the presence of viscous friction forces, and $S_e$ is the three-dimensional energy liberation, which appears from the work of frictional forces $\mu_{\sum} D$ (where $D$ is the dissipation function), of heat transfer by heat conduction processes $div\left(\lambda_{\sum} gradT\right)$ and energy liberation $Q_L$, caused by the laser's radiation action on the plasma of the environment and the vapors of the barrier material. Re is the Reynolds number, Pr is the Prandtl number, $u(r,z,t), v(r,z,t)$ are projections of the velocity vector $\vec{V}(r,z,t)$ on axes $R$ and $Z$, $e$ is the specific internal energy of plasma, $J = \partial(r,z)/\partial(\xi,\eta)$ is the Jacobian transition from a cylindrical coordinate system $r$, $z$ to the curvilinear coordinates $\xi, \eta$, $V_\xi = \xi_r u + \xi_z \mathrm{v}$, $V_\eta = \eta_r u + \eta_z v$ are the contravariant components of the velocity vector $\vec{V}$ in the curvilinear coordinates $\xi$, $\eta$, $\rho$, $P$ are the plasma density and pressure, and $\sum_i q_{i\xi}, \sum_i q_{i\eta}$ are projections of the flux density vector of radiant energy $\vec{q}$ on the axis of curvilinear coordinates $\xi$ and $\eta$, $\alpha = 0$ corresponding to the plane flow, $\alpha = 1$ corresponding to axially symmetric flow.

Hydrogen oxidation is considered as a multi-stage process described by nine chemical equations: $H_2 + O_2 = 2OH$, $H_2 + M = 2H + M$, $H_2O + M = OH + H + M$, $H_2O + O = 2OH$, $O_2 + M = 2O + M$, $OH + M = H + O + M$, $O_2 + H = OH + O$, $H_2 + O = OH + H$, and $H_2O + H = OH + H_2$.

To determine the ablating vapor's plasma density of a metal barrier material $\rho_g \in [0,1]$ in the system of the above equations we add an additional continuity equation: $\frac{\partial \rho_g}{\partial t} + \vec{V}\nabla\rho_g = 0$. This equation allows us to determine the spatial position of the contact boundary, which separates the 'boundary' of the ablating vapors of the metal barrier material from the ambient gas. When a laser radiation with a flux density of $10^9$ W cm$^{-2}$ acts on the target, the magnetic field will be due to thermal EMF. In this case, the main mechanism is the generation's gradient of the magnetic field, when the eddy currents in the plasma are formed as a result of the noncollinearity of electron concentration gradients $\nabla n_e$ and the temperature $\nabla T$.

The equation of the magnetic field's generation $\vec{B}$, taking into account the source of the magnetic field in the laser plasma and the superposition principle, is:

$$\frac{\partial \vec{B}}{\partial t} = rot\left[\vec{V} \times \vec{B}\right] - \frac{c^2}{4\pi}\frac{t_*}{L_*^2} rot\left(\frac{rot\vec{B}}{\sigma}\right) - P_g,$$
$$P_g = \frac{t_*}{B_* L_*^2}\frac{ck}{en_e}\left[\nabla n_e \times \nabla T\right],$$

where $n_e$ is the electron concentration, and $T$ is the temperature of a laser flare's plasma.

The radiation transfer equation is represented in the form of an equation system for the diffusion many-group approximation [5]:

$$\frac{1}{J}\frac{\partial\left(Jq_{i\xi}\right)}{\partial \xi} + \frac{1}{J}\frac{\partial\left(Jq_{i\eta}\right)}{\partial \eta} + \chi_i c U_i = 4\chi_i \sigma_i T^4,$$
$$\frac{c}{3}\frac{\partial U_i}{\partial \xi} + \chi_i q_{i\xi} = 0, \quad \frac{c}{3}\frac{\partial U_i}{\partial \eta} + \chi_i q_{i\eta} = 0,$$

where $U_i(y,z,t)$ is the radiant energy density in the $i$th spectral group, and $\chi_i$ is the spectral absorption coefficient.

A system of equations describing the processes of heating and the surface material's evaporation of a metal wall under the influence of thermal radiation from a plasma volume with a radiation flux density $q$ (which takes into account the laser radiation incident on the wall $q_{las}$), without taking into account the hydrodynamic processes in a condensed medium, consists of a quasi-one-dimensional heat equation in a moving (connected with the front of the evaporation wave) coordinate system with an axis $r$, which is perpendicular to the evaporation surface:

$$\frac{\partial T_s}{\partial t} = a_M \frac{\partial^2 T_s}{\partial r^2} + V_0 \frac{\partial T_s}{\partial r}$$

with initial and boundary conditions:

$$k_m \frac{\partial T_s}{\partial r}(0,t) = q_{laz}(0,t) - L_v \rho(0,t)\,\mathrm{v}(0,t),$$
$$T_s(z \to \infty, t) = T_0, \quad T_s(0, t=0) = T_0,$$

and an equation system that determines the evaporation kinetics of the condensed matter's surface within the framework of the Knudsen layer model [6]:

$$\frac{T(0,t)}{T_s(0,t)} = \left[\sqrt{1+\pi\left(\frac{(\gamma-1)m}{(\gamma+1)2}\right)^2} - \sqrt{\pi}\frac{\gamma-1}{\gamma+1}\frac{m}{2}\right]^2,$$

$$\frac{\rho(0,t)}{\rho_s(0,t)} = \sqrt{\frac{T_s(0,t)}{T(0,t)}}\left[\left(m^2+\tfrac{1}{2}\right)e^{m^2}erfc\,(m) - \frac{m}{\sqrt{\pi}}\right] + \tfrac{1}{2}\frac{T_s(0,t)}{T(0,t)}\left[1-\sqrt{\pi}me^{m^2}erfc\,(m)\right],$$

$$p_s(t) = p_1\exp\left[\frac{\Im L_v}{RT_1}\left(1-\frac{T_1}{T_s(0,t)}\right)\right],$$

$$m = \frac{V(0,t)}{\sqrt{2RT(0,t)/\Im}}, \quad \rho(0,t)\,v(0,t) = \rho_m V_0.$$

Here $T_s(r,z,t)$ is the temperature of the condensed medium at the point $(z,\ t)$, $a_m$, $k_m$, $\rho_m$ are the coefficients of heat diffusivity, thermal conduction and density of the material; $V_0$ is the evaporation velocity; $P_s, \rho_s$ are the pressure and density of a condensed substance's saturated vapor at the surface temperature $T_s(z=0,r,t)$; $R$ is the universal gas constant; $T_1$ is the value of the condensed medium's surface temperature, which corresponds to the saturated vapor pressure $p_1$, $L_v$ is the latent heat of vaporization; $\Im$ is the molar mass of the vapor; $T(0,t), \rho(0,t), V(0,t)$ are the temperature, density, and velocity of the plasma at the outer boundary of the Knudsen layer at the point $(z=0,r)$ at the time $t$; $\gamma$ is the adiabatic exponent of condensed matter vapors.

The absorption coefficient of laser radiation for a $CO_2$ laser and *Nd* laser in the air plasma is found using the formulas given in [7].

Calculation of the equation system of optical $\chi_i(T,\rho)$ with characteristics of working mediums was carried out using the computer system ASTEROID [8]. In calculating the optical characteristics, the entire spectrum was divided into seven groups with interval boundaries [0, 1–3, 14–5, 98–6, 52–7, 95–9, 96–18, 6–200] eV, for air.

Turbulent viscosity coefficients $\mu_\sum$ and $\lambda_\sum$ and thermal conduction are calculated using equations $q-\omega$ of the Coacley model in a curvilinear coordinate system $\xi, \eta$ [9].

## 3. Method of numerical simulation

The numerical solution developed in the work of the nonstationary two-dimensional radiation-gas dynamic model is based on the method of splitting by physical processes and spatial directions. In this case, the solution of a 2D nonstationary equation system for viscous single-temperature radiation plasma dynamics, written in a vector semi-divergent form in the curvilinear coordinate system $\xi, \eta$, is as follows:

$$\frac{\partial\vec{U}}{\partial t} + \frac{\partial\vec{F}}{\partial\xi} + \frac{\partial\vec{G}}{\partial\eta} + \vec{S} = \frac{1}{\mathrm{Re}}\left[\frac{\partial\vec{F}_v}{\partial\xi} + \frac{\partial\vec{G}_v}{\partial\eta} + \vec{S}_v\right].$$

The vectors in this equation system have the form:

$$\vec{U} = J\begin{Vmatrix}\rho_i\\ \rho\\ \rho u\\ \rho v\\ \rho e\\ \rho q\\ \rho\omega\end{Vmatrix},\quad \vec{F} = J\begin{Vmatrix}\rho_i V_\xi\\ \rho V_\xi\\ \rho u V_\xi\\ \rho v V_\xi\\ \rho e V_\xi\\ \rho q V_\xi\\ \rho\omega V_\xi\end{Vmatrix},\quad \vec{G} = J\begin{Vmatrix}\rho_i V_\eta\\ \rho V_\eta\\ \rho u V_\eta\\ \rho v V_\eta\\ \rho e V_\eta\\ \rho q V_\eta\\ \rho\omega V_\eta\end{Vmatrix},$$

$$\vec{S} = J\begin{Vmatrix}\alpha\frac{\rho c_i u}{r} + Div\left(\rho D_i\nabla c_i\right)\\ \alpha\frac{\rho u}{r}\\ \xi_r\frac{\partial P}{\partial\xi} + \eta_r\frac{\partial P}{\partial\eta} + \alpha\frac{\rho u^2}{r}\\ \xi_z\frac{\partial P}{\partial\xi} + \eta_z\frac{\partial P}{\partial\eta} + \alpha\frac{\rho uv}{r}\\ \frac{P}{J}\left\{\frac{\partial(JV_\xi)}{\partial\xi} + \frac{\partial(JV_\eta)}{\partial\eta}\right\} + \alpha\frac{Pu}{r} + \alpha\frac{\rho eu}{r} - \frac{t_*}{\rho_* e_*}Q_L - D\\ \alpha\frac{\rho qu}{r} - \frac{\rho q}{2\omega_*\omega}\left(C_\mu fD\left[\frac{V_*}{L_*}\right]^2 - \frac{2}{3}\omega_*\frac{V_*}{L_*}\omega div\vec{V} - \omega_*^2\omega^2\right)\\ \alpha\frac{\rho\omega u}{r} - \frac{\rho}{\omega_*}\left(C_1\left(C_\mu D\left[\frac{V_*}{L_*}\right]^2 - \frac{2}{3}\omega_*\frac{V_*}{L_*}\omega div\vec{V}\right) - C_2\omega_*^2\omega^2\right)\end{Vmatrix}$$

$$\vec{F}_v = J\begin{Vmatrix}0\\ 0\\ \xi_r\sigma_{rr} + \xi_z\sigma_{rz}\\ \xi_r\sigma_{zr} + \xi_z\sigma_{zz}\\ \frac{\gamma}{\mathrm{Pr}}\left\{\lambda_\sum\left(\xi_r^2+\xi_z^2\right)T_\xi + \lambda_\sum\left(\xi_r\eta_r + \xi_z\eta_z\right)T_\eta\right\}\\ \mu_\sum q\left(\xi_r^2+\xi_z^2\right)q_\xi + \mu_\sum q\left(\xi_r\eta_r+\xi_z\eta_z\right)q_\eta\\ \mu_\sum\omega\left(\xi_r^2+\xi_z^2\right)\omega_\xi + \mu_\sum\omega\left(\xi_r\eta_r+\xi_z\eta_z\right)\omega_\eta\end{Vmatrix},$$

$$\vec{G}_v = J\begin{Vmatrix}0\\ 0\\ \eta_r\sigma_{rr} + \eta_z\sigma_{rz}\\ \eta_r\sigma_{zr} + \eta_z\sigma_{zz}\\ \frac{\gamma}{\mathrm{Pr}}\left\{\lambda_\sum\left(\eta_r\xi_r + \eta_z\xi_z\right)T_\xi + \lambda_\sum\left(\eta_r^2+\eta_z^2\right)T_\eta\right\}\\ \mu_\sum q\left(\eta_r\xi_r+\eta_z\xi_z\right)q_\xi + \mu_\sum q\left(\eta_r^2+\eta_z^2\right)q_\eta\\ \mu_\sum\omega\left(\eta_r\xi_r+\eta_z\xi_z\right)\omega_\xi + \mu_\sum\omega\left(\eta_r^2+\eta_z^2\right)\omega_\eta\end{Vmatrix},$$

$$\vec{S}_v = J\begin{Vmatrix}0\\ 0\\ \alpha\frac{2\mu_\sum\left[\xi_r\frac{\partial u}{\partial\xi} + \eta_r\frac{\partial u}{\partial\eta}\right] - 2\alpha\mu_\sum\frac{u}{r}}{r}\\ \alpha\frac{\sigma_{rz}}{r}\\ \alpha\frac{\gamma}{\mathrm{Pr}}\frac{\lambda_\sum}{r}\left\{\xi_r\frac{\partial T}{\partial\xi} + \eta_r\frac{\partial T}{\partial\eta}\right\} + \mu_\sum D\\ \alpha\frac{\mu_\sum q}{r}\left\{\xi_r\frac{\partial q}{\partial\xi} + \eta_r\frac{\partial q}{\partial\eta}\right\}\\ \alpha\frac{\mu_\sum\omega}{r}\left\{\xi_r\frac{\partial\omega}{\partial\xi} + \eta_r\frac{\partial\omega}{\partial\eta}\right\}\end{Vmatrix}.$$

At the first time fractional step $t\in[t, t+\Delta t/3]$, using the explicit integro–interpolation method and the corresponding boundary conditions, the 'hyperbolic' ('inviscid') part of the equation system is solved. We use the nonlinear quasimonotone compact polynomial difference scheme of improved accuracy [10, 11], which in the spatially smooth part of the numerical solution allows us to achieve the seventh order of accuracy:

$$\frac{\partial \vec{U}_{i,j}}{\partial t}+\frac{\vec{F}_{i+1/2,j}-\vec{F}_{i-1/2,j}}{\Delta\xi}+\frac{\vec{G}_{i,j+1/2}-\vec{G}_{i,j-1/2}}{\Delta\eta}+\vec{S}_{i,j}=0.$$

For the 'hyperbolic' (convective heat transfer) part of the equation system, the nonlinear quasimonotone compact polynomial difference scheme is developed in the work with an increased order of accuracy:

$$\frac{\partial \vec{U}_i}{\partial t}+\frac{F\left(\vec{U}_{i+1/2}\right)-F\left(\vec{U}_{i-1/2}\right)}{\Delta_\xi}=\overrightarrow{F_2},$$
$$\Delta_\xi=\left[\xi_{i-1/2}-\xi_i,\xi_{i+1/2}-\xi_i\right].$$

The gas-dynamic parameters $U_i^{n+1}, U_i^n$ refer to the centers of the calculated cells, while the flows on the surface of those cells $(F_{i\pm1/2}^n)$ need to be determined. In order to increase the order of approximation of the difference scheme, it is necessary to 'restore' the gas dynamic parameters $Y_{i\pm1/2}^{R,L}$ 'right' (index $R$) and 'left' (index $L$) from the boundaries of the calculated cells. The reconstructed function, $Y(\xi),\xi\in\left[-\frac{\Delta_\xi}{2},\frac{\Delta_\xi}{2}\right]$, can be represented in the form of the $i$th polynomial of the seventh degree (in this case a nonlinear quasimonotone compact polynomial difference scheme with higher order of accuracy is used):

$$\begin{aligned}Y(\xi)=F_i^n(\xi)=Y_i+\phi(Y_i)\left(\frac{\partial Y}{\partial\xi}\right)_i[\xi-\xi_i]\\+\frac{\phi(Y_i)}{2!}\left(\frac{\partial^2 Y}{\partial\xi^2}\right)_i[\xi-\xi_i]^2++a_i[\xi-\xi_i]^3+b_i[\xi-\xi_i]^4\\+c_i[\xi-\xi_i]^5+d_i[\xi-\xi_i]^6+e_i[\xi-\xi_i]^7,\end{aligned}$$

where the function $\phi(Y)$ is the limiter [10, 11]. The function $Y(x)$ satisfies the conditions of smooth conjugation and the condition of conservativeness:

$$F_i^n(\xi_{i-1})=Y_{i-1}^n,\quad F_i^n(\xi_{i+1})=Y_{i+1}^n,\quad \frac{dF_i^n(\xi_{i-1})}{d\xi}=Y_{\xi,i-1}^n,$$
$$\frac{dF_i^n(\xi_{i+1})}{d\xi}=Y_{\xi,i+1}^n,\quad \frac{1}{\Delta_\xi}\int_{-\frac{\Delta_\xi}{2}}^{+\frac{\Delta_\xi}{2}}Y_i^n(\xi)d\xi=Y(\xi_i).$$

The above conditions for smooth conjugation can be formulated as a linear algebraic equation system:

$$A\overrightarrow{Z_i}=\overrightarrow{F_i},\quad \overrightarrow{Z_i}=(a_i,b_i,c_i,d_i,e_i)^T,\ \overrightarrow{F_i}=(F_1,F_2,F_3,F_4,F_5)^T,$$
$$A=\begin{pmatrix}-\Delta_\xi{}^3 & \Delta_\xi{}^4 & -\Delta_\xi{}^5 & \Delta_\xi{}^6 & -\Delta_\xi{}^7\\ 3\Delta_\xi{}^2 & -4\Delta_\xi{}^3 & 5\Delta_\xi{}^4 & -6\Delta_\xi{}^5 & 7\Delta_\xi{}^6\\ \Delta_\xi{}^3 & \Delta_\xi{}^4 & \Delta_\xi{}^5 & \Delta_\xi{}^6 & \Delta_\xi{}^7\\ 3\Delta_\xi{}^2 & 4\Delta_\xi{}^3 & 5\Delta_\xi{}^4 & 6\Delta_\xi{}^5 & 7\Delta_\xi{}^6\\ 0 & \frac{1}{5}\left(\frac{\Delta_\xi}{2}\right)^4 & 0 & \frac{1}{7}\left(\frac{\Delta_\xi}{2}\right)^6 & 0\end{pmatrix},$$
$$F_1=Y_{i-1}^n-Y_i+\phi(Y_i)\left(\frac{\partial Y}{\partial\xi}\right)_i\Delta_\xi-\frac{\phi(Y_i)}{2!}\left(\frac{\partial^2 Y}{\partial\xi^2}\right)_i\Delta_\xi^2,$$
$$F_2=Y_{\xi,i-1}^n-\phi(Y_i)\left(\frac{\partial Y}{\partial\xi}\right)_i+\phi(Y_i)\left(\frac{\partial^2 Y}{\partial\xi^2}\right)_i\Delta_\xi,$$
$$F_3=Y_{i+1}^n-Y_i-\phi(Y_i)\left(\frac{\partial Y}{\partial\xi}\right)_i\Delta_\xi-\frac{\phi(Y_i)}{2!}\left(\frac{\partial^2 Y}{\partial\xi^2}\right)_i\Delta_\xi^2,$$
$$F_4=Y_{\xi,i+1}^n-\phi(Y_i)\left(\frac{\partial Y}{\partial\xi}\right)_i-\phi(Y_i)\left(\frac{\partial^2 Y}{\partial\xi^2}\right)_i\Delta_\xi,\quad F_5=-\frac{\phi(Y_i)}{3!}\left(\frac{\partial^2 Y}{\partial\xi^2}\right)_i\left[\frac{\Delta_\xi}{2}\right]^2.$$

The spatial derivatives $\left(\frac{\partial Y}{\partial\xi}\right)_{i,j}$, entering into piecewise polynomial distributions $Y(\xi)$, are calculated as follows. For the discrete function $Y_i$ we determine the approximate value of $F_i$ of the first partial derivative with respect to the space variable $\xi$ with an eighth order of accuracy [12, 13]. For this, in each cell with the number $i$, for each recoverable value $Y_{i,j}$ the calculation of the nonmonotonicity index is performed $Ind(Y)$:

$$\begin{aligned}Ind_1&=\tfrac{1}{12}\left|-Y_{i+2,j}+16Y_{i+1,j}-30Y_{i,j}+16Y_{i-1,j}-Y_{i-2,j}\right|,\\Ind_2&=\tfrac{1}{2}\left|-Y_{i+2,j}+4Y_{i+1,j}-3Y_{i,j}\right|,\\Ind_3&=\tfrac{1}{2}\left|3Y_{i,j}-4Y_{i-1,j}+Y_{i-2,j}\right|,\\Ind(Y)_i&=\tfrac{Ind_1}{(Ind_2+Ind_3+\theta)},\end{aligned}$$

where the value $\Theta$ is the small parameter.

Then we find the first derivative $f$ with respect to the variable $\xi$ by the usual approximation formula with the second order of accuracy, and we perform its 'monotonic restriction' on the grid:

$$\begin{aligned}&\overline{Ind}(Y)_i=1\cdot Ind(Y)_i+2\cdot\left[1-Ind(Y)_i\right],\ f_i=\tfrac{Y_{i+1}-Y_{i-1}}{2\Delta_\xi}+O\left(\Delta_\xi{}^2\right),\\&Ind_R=\left(\overline{Ind}(Y)_{i+2}\left|f_{i+2}\right|,\overline{Ind}(Y)_{i+1}\left|f_{i+1}\right|\right),\\&Ind_L=\left(\overline{Ind}(Y)_{i-1}\left|f_{i-1}\right|,\overline{Ind}(Y)_{i-2}\left|f_{i-2}\right|\right),\\&\tilde{f}_i=sign(Y_{i+1}-Y_{i-1})\cdot\min\left(Ind_R,\left|f_i\right|,Ind_L\right),\end{aligned}$$

where $\Delta$ is the width of the spatial grid in the direction $\xi$. Then the approximate 'monotonized' value of $\tilde{F}_i$ the first partial derivative with respect to the space variables $\xi$ with the error of approximation $O\left(\Delta_\xi{}^6\right)$ can be found by solving the equation system with a tridiagonal matrix:

$$\begin{aligned}&\widetilde{F_i}=\left\{\left(E+\tfrac{\Delta_2}{6}\right)^{-1}Q_i\right\}_i,\ Q_i=\left(E+\tfrac{\Delta_2}{30}\right)\tilde{f}_i\\&Ind_R=\left(\overline{Ind}(Y)_{i+2}\left|\tilde{F}_{i+2}\right|,\overline{Ind}(Y)_{i+1}\left|\tilde{F}_{i+1}\right|\right),\\&Ind_L=\left(\left|\tilde{F}_{i+1}\right|,\overline{Ind}(Y)_{i-1}\left|\tilde{F}_{i-1}\right|,\overline{Ind}(Y)_{i-2}\left|\tilde{F}_{i-2}\right|\right),\\&\tilde{f}_i=\mathrm{sign}(Y_{i+1}-Y_{i-1})\cdot\min\left(Ind_R,\left|\tilde{F}_i\right|,Ind_L\right),\end{aligned}$$

where $\Delta_0 f_i=f_{i+1}-f_{i-1}$, $\Delta_2 f_i=f_{i+1}-2f_i+f_{i-1}$, and $E$ is the unity operator.

This method of calculating the first derivative $F_i$ is used in the formation of boundary conditions in the case of an approximate 'monotonized' value of$\tilde{F}_i$, the first partial derivative with respect to the space variable $\xi$ with the error of approximation $O\left(\Delta_\xi{}^8\right)$. In this case, calculations should be carried out on the basis of solving the equation system with a five-diagonal matrix [12, 13]:

$$F_i=\left\{\left(E+\frac{2\Delta_2}{7}+\frac{\Delta_2^2}{70}\right)^{-1}Q_i\right\}_i,\quad Q_i=\left(E+\frac{5\Delta_2}{42}\right)\tilde{f}_i.$$

Spatial second-order derivatives are determined from formulas [12–14]. By means of the reconstructed function $Y(\xi)$ the gas dynamic parameters are 'recoverable'; $Y_{i\pm1/2}^{R,L}$ 'on the right' (index—$R$) and 'on the left' (index—$L$) from the border of computation cells. Then, 'diffusion-resistant' correction of the 'recoverable' parameters $Y(\xi)$ at the edges of the cell $Y_{i\pm1/2}^{R,L}$ [15, 16] is completed. In order to reduce the amplitude of the 'parasitic' oscillations of the numerical solution in the initial function's neighborhood of discontinuities,

it can be expanded in a Lagrange–Burman series in powers of a certain monotonic function [17, 18].

For example, by function $f(\xi)$:

$$f(\xi) = \Delta_\xi th\left(\frac{\beta}{\Delta_\xi}(\xi - \xi_i)\right),$$

$$\beta = 4 \cdot Ind(Y) + 6 \cdot (1 - Ind(Y)), \left(\frac{\partial f}{\partial \xi}\right)_i \neq 0.$$

Then, for the reconstructed function $Y(\xi)$ near strong discontinuities the conditions of the conjugation and persistence can be written in the form of a system (analogous to that formulated above) of linear algebraic equations [11]. The remaining details of the nonlinear quasimonotone compact-polynomial difference scheme are given in [10, 11]. The proposed difference scheme is a further development of WENO [19].

The above differential system of equations relative to the time variable $t$ is a system of ordinary differential first-order equations which can be solved with the help of a multi-step Runge–Kutta method (in this paper we use the three-step version of the method). At the second time fractional step $t \in [t + \Delta t/3, t + 2\Delta t/3]$ we use an explicit method using the boundary conditions of 'sticking', and the 'parabolic' ('viscous') part of the equation system. In this case, the first and the second order derivatives included in the system of equations of the second time fractional step under consideration were found using the compact scheme, with sixth order of accuracy. At the third time fractional step $t \in [t + 2\Delta t/3, t + \Delta t]$, the 'hard' part of the $q - \omega$ Coacley's model is calculated using the implicit Rosenbrock method.

Time step $\Delta t$, necessary for integrating the above-mentioned difference scheme, is chosen from the condition that the Courant–Friedrichs–Levy stability criterion is performed [10]. When solving the radiation transfer equations, the modified alternating-triangular method is applied using a three-layer iterative scheme in which the iterative 'time' step is found using the conjugate direction method [20, 21]. The combustion process of hydrogen–oxygen mixtures is described by the corresponding equations of chemical kineticism, which are solved by the Rosenbrock method, which makes it possible to overcome 'rigidity' of this system of equations.

## 4. Results of calculations

In our numerical experiments we will give an initial assessment of the possibility of intensifying the mixing and ignition of a hydrogen–oxygen mixture by laser plasma in the channel of the engine of a prospective aircraft. In this case powerful radiation, turbulent mixing and shock waves can initiate combustion processes in a mixture of oxygen and hydrogen. Now we discuss the results of numerical modeling of optical-included breakdown and the possibility of igniting a stationary and moving hydrogen–oxygen mixture near a flat stationary aluminum barrier when exposed to the laser radiation fluxes of a $CO_2$ laser (10.6 $\mu$m) and ambient air pressure of 1 atm. We note that the numerical modeling of this task is

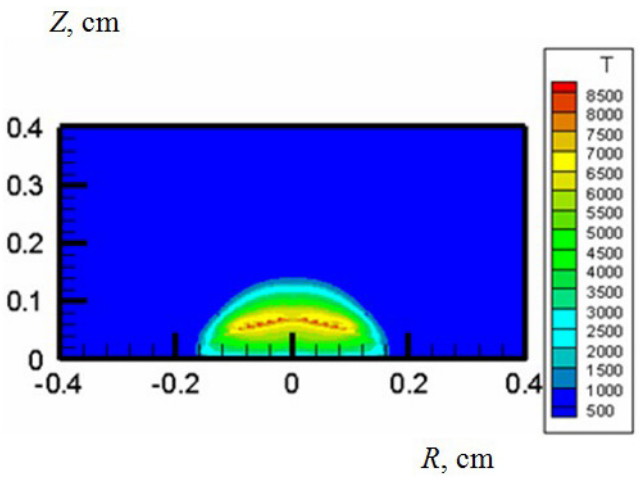


**Figure 1.** The spatial temperature distribution $T$ [K] in the laser flare at the time $t = 1.6$ $\mu$s.

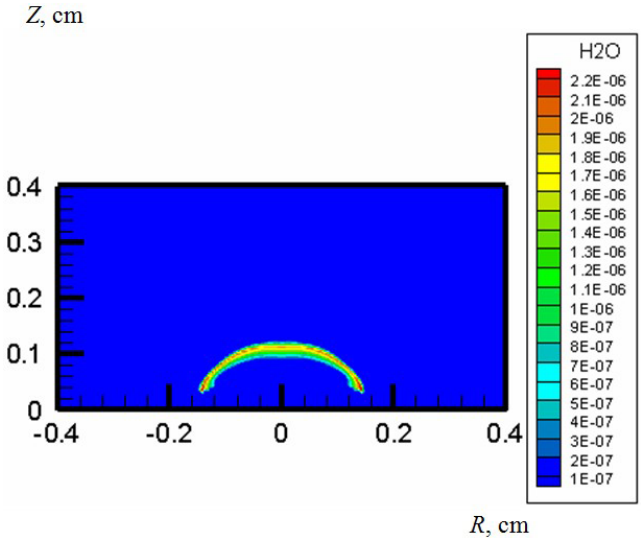


**Figure 2.** The spatial distribution of the molar concentration of $H_2O$ at the time $t = 1.6$ $\mu$s.

rather complicated; for example, the high rigidity of the chemical kinetic equations, etc. The sharp temperature dependence of the rate of chemical reactions, and a strong change in the density of the gas mixture due to a change in the average molecular weight, also add to the complexity. To overcome these difficulties both significant computing power and development of special algorithms are required.

We present a scheme consisting of eight reactions as a model of hydrogen–air mixture combustion. The scheme is a reduction of the model consisting of 25 reactions and described in [22]. The constants of these reactions are also taken from [22]. The influence of the choice of the kinetic model on the combustion of the mixture is also discussed there. The formation rate of the component is determined by the law of mass action:

$$W_k = \sum_{r=1}^{N_r} (b_{rk} - f_{rk}) \left[ k_{fr} \prod_s \left(\frac{\rho Y_s}{m_s}\right)^{f_{rk}} - k_{br} \prod_s \left(\frac{\rho Y_s}{m_s}\right)^{f_{br}} \right].$$

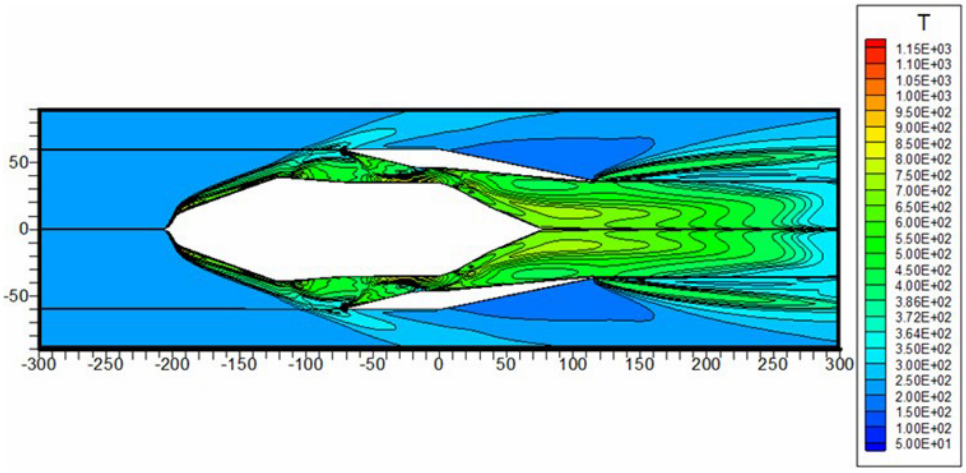


**Figure 3.** Spatial temperature distributions $T$ [K] in the geometric model of HEG.

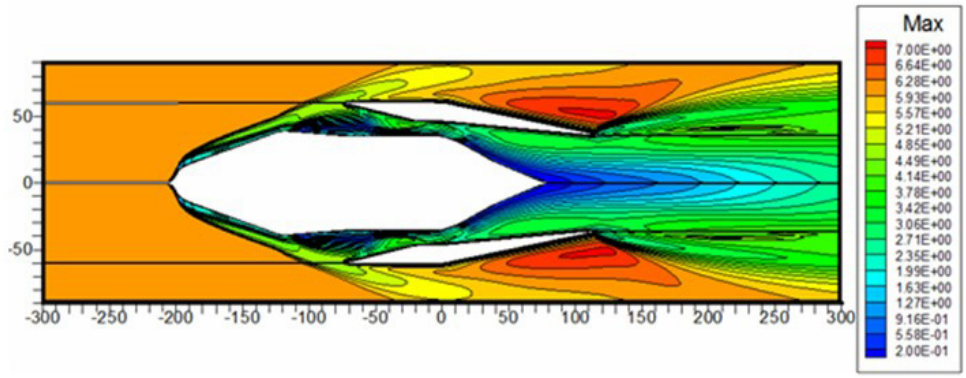


**Figure 4.** Spatial distributions of the Mach number in the geometric model of HEG.

The rates of the forward $f_{rk}$ and counter $b_{rk}$ reactions are given by the Arrhenius formula:

$$k_f = A_f T^{P_f} e^{-E_f/RT}, \quad k_b = A_b T^{P_b} e^{-E_b/RT}.$$

Specific calculations were made for the cases of the pulses' action of the rectangular shape laser radiation with a pulse duration of 10–1000 ns. The value of the total energy of laser radiation was 0.1–3 J, and the size of the focusing spot was ~100–500 $\mu$m. The material of the metal barrier in the computation research was Al. The ambient was a hydrogen–oxygen mixture.

Figures 1 and 2 show the structure of the laser plasma, and the combustion region an initially immobile ($W_\infty = 0$) hydrogen–oxygen mixture at time $t = 1.6$ $\mu$s. The combustion of the hydrogen–oxygen mixture at this time is observed in the region located between the contact boundary and the front shock wave.

We intensify the combustion process of the oxyhydrogen mixture under the action of laser radiation by an additional action: the leakage of a supersonic air stream compressed into the air, taken into the plasma formation of the near-surface laser plasma.

To do this, we perform a numerical analysis of the possibility of ignition of the hydrogen–oxygen combustible mixture that moves in the engine channel of a prospective aircraft. At the same time, we will concentrate on reproducing only the

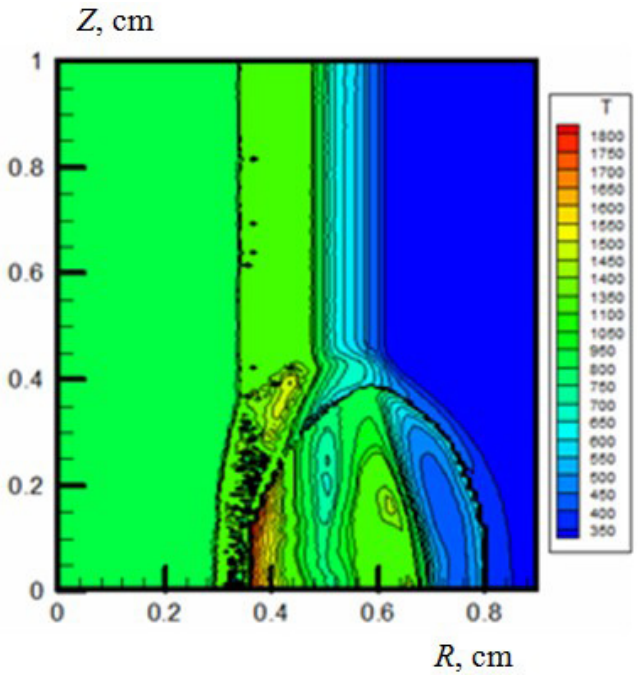


**Figure 5.** The structure of the temperature field of the laser flare and the combustion field of a hydrogen–oxygen mixture under laser action at $t = 4.18$ $\mu$s.

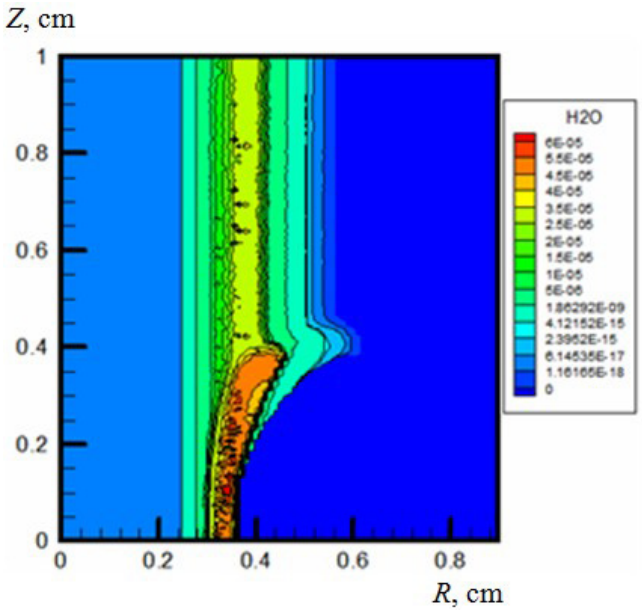


**Figure 6.** The structure of the field of the molar concentration of the $H_2O$ laser flare and the combustion field of oxyhydrogen mixture under laser action at $t = 4.18$ $\mu$s.

key characteristics of the operation of the hypersonic plane (HP), therefore, as the simplest version of HP, we will consider the high enthalpy shock tunnel Göttingen (HEG) [23].

When calculating the gas dynamic parameters of the flow in the channel of the HEG [23] at the boundary of the calculated region (figures 3 and 4), through which the undisturbed airflow enters, the following parameters were set: $\gamma = 1.4, T_\infty = 223$ K, $P_\infty = 2060$ Pa, $W_\infty = 1860$ cm s$^{-1}$, where $W_\infty$, $T_\infty$, $P_\infty$ are the velocity, temperature, and pressure of the air flow coming through the boundary surface, respectively. From the calculations of the gas dynamic parameters of the flow in the channel of the HEG [23], it follows that the gas-dynamic parameters of the air compressed in the air intake and flowing onto the injection area of fuel in the HEG have the following range of values: $P = 1 \div 2$ atm, $T = 0{,}3 \div 1$ K, and Mach number $M = 2$.

Figures 3–6 show the structure of the laser flare temperature field and the combustion field of the hydrogen–oxygen mixture. The parameters of the laser action are $t_{las} = 50$ $\mu$s, $q_{las} = 2 \cdot 10^7$ W cm$^{-2}$.

It follows (from figure 1 and the results of calculations in a stationary ambient) that when the external gas flow leaks into the laser flare in the interaction region, the pressure increases four-fold, and the molar concentration of $H_2O$ increases approximately twenty-fold compared to the stationary gas ambient.

The calculations performed in this work allow us to hope that the proposed approach (ignition of oxyhydrogen mixture by erosive laser flame) can be used for extreme ignition of a combustible mixture in prospective aircraft engines.

## 5. Conclusion

A mathematical model of a near-surface laser flare is developed, based on the equations of radiation plasma dynamics written in arbitrary curvilinear coordinates. For numerical resolution of the 'hyperbolic' part of the system of Reynolds equations, a nonlinear quasimonotone compact-polynomial difference scheme of an increased accuracy order is applied. This computational scheme is designed for a wide range of physical and technical problems: technical systems with a high energy density (due to the fusion reaction), based on magneto-inertial confinement (due to superstrong magnetic fields); pulse radiation-magneto gas-dynamic systems designed to initiate extreme ignition of fuel mixtures in the working channel of the engine of prospective aircraft; the design determination of the characteristics of high-brightness plasma radiation sources and shock wave generators. The calculations of all the main gas-dynamic and radiative parameters of a laser flare and a metal barrier have been performed. Numerical calculations of laser-stimulated combustion of a hydrogen–oxygen mixture have also been performed.

## Acknowledgments

This research was supported by the Ministry of Science and Higher Education of the Russian Federation (13.5240.2017/8.9).

## References

[1] Schwarz E, Muri I, Tauer J, Kofler H and Wintner E 2010 Laser-induced ignition by optical breakdown *Laser Phys.* **20** 1545–53
[2] Gvozdev S V *et al* 2017 Remote processing of metals with laser radiation with increased intensity *Inorg. Mater.: Appl. Res.* **8** 795–801
[3] Surzhikov S T, Kuzenov V V and Petrusev A S 2008 Radiation gas dynamics of aluminium laser plume in air *AIAA* p 1108
[4] Benavides O, De La Cruz May L, Mejia E B, Ruz Hernandez J A and Flores Gil A 2016 Laser wavelength effect on nanosecond laser light reflection in ablation of metals *Laser Phys.* **26** 126101
[5] Surzhikov S T 2013 *Computational Physics of Electric Discharges in Gas Flows* (Berlin: de Gruyter & Co) p 427
[6] Knight C J 1979 Theoretical modeling of rapid surface vaporization with back pressure *AIAA J.* **17** 519–23
[7] Raizer Yu P 1991 *Gas Discharge Physics* (Berlin: Springer)
[8] Surzhikov S T 2003 Computing system for solving radiative gas dynamic problems of entry and re-entry space vehicles *Proc. of the 1st Int. Workshop on Radiation of High Temperature Gases in Atmospheric Entry* vol ESA-533 pp 111–8
[9] Coacley T J 1983 Turbulence modeling methods for the compressible Navier-Stokes equations *AIAA* p 1693
[10] Kuzenov V V 2017 Computer simulation of compression and energy release upon laser irradiation of cylindrically symmetric target *Phys. At. Nuclei* **80** 1683–6
[11] Kuzenov V V and Ryzhkov S V 2018 Numerical modeling of laser target compression in an external magnetic field *Math. Models Comput. Simul.* **10** 255–64
[12] Savel'ev A D 2007 High-order composite compact schemes for simulation of viscous gas flows *Comput. Math. Math. Phys.* **47** 1332–46

[13] Ryzhkov S V and Kuzenov V V 2019 Analysis of the ideal gas flow over body of basic geometrical shape *Int. J. Heat Mass Transfer* **132** 587–92
[14] Dovgilovich L E and Sofronov I L 2015 High-accuracy finite-difference schemes for solving elastodynamic problems in curvilinear coordinates within multiblock approach *Appl. Numer. Math.* **93** 176–94
[15] Kuzenov V V and Ryzhkov S V 2017 Numerical simulation of the effect of laser radiation on matter in an external magnetic field *J. Phys.: Conf. Ser.* **830** 012124
[16] Xu Z and Shu C-W 2006 Anti-diffusive finite difference WENO methods for shallow water with transport of pollutant *J. Comput. Math.* **24** 239–51
[17] Kuzenov V V and Ryzhkov S V 2017 Approximate method for calculating convective heat flux on the surface of bodies of simple geometric shapes *J. Phys.: Conf. Ser.* **815** 012024
[18] Vorozhtsov E V 2010 Derivation of explicit difference schemes for ordinary differential equations with the aid of Lagrange–Burmann expansions *Lect. Notes Comput. Sci.* **6244** 250–66
[19] Shu C-W 1997 Essentially non-oscillatory and weighted essentially non-oscillatory schemes for hyperbolic conservation laws *Technical Reports NASA* Report No. 65–97
[20] Samarskii A A and Nikolaev E S 1989 *Numerical Methods for Grid Equations* (Basel: Birkhauser) 242p
[21] Ryzhkov S V and Kuzenov V V 2019 New realization method for calculating convective heat transfer near the hypersonic aircraft surface *ZAMP* **70** 46
[22] Evans J S and Schexnayder C J 1980 Influence of chemical kinetics and unmixedness on burning in supersonic hydrogen flames *AIAA J.* **18** 188–93
[23] Steelant J *et al* 2006 Comparison of supersonic combustion tests with shock tunnels, flight and CFD *42nd AIAA/ASME/SAE/ASEE Joint Propulsion Conf. & Exhibition* pp 2006–4684